Materials Today Communications 51 (2026) 114653

Contents lists available at ScienceDirect

Materials Today Communications

journal homepage: www.elsevier.com/locate/mtcomm

Precursor concentration-tuned optical and electrochromic performance of sol-gel-derived V_2O_5 thin-film devices

Gregory Soon How Thien [a], Zhang-Xuan Cheng [b,c], Ming-Yue Tan [b], Cheikh Zakaria Eldjilali [b], Abdelrahman Hamed Ebrahem Abdelhamed [b], Faisal Abdullah Sadeq [b], Pei-Ling Low [a,b], Kar Ban Tan [d], Kah-Yoong Chan [a,b,*]

[a] Centre for Advanced Devices and Systems, Centre of Excellence for Robotics and Sensing Technologies, Multimedia University, Persiaran Multimedia, Cyberjaya, Selangor 63100, Malaysia
[b] Faculty of Artificial Intelligence and Engineering, Multimedia University, Persiaran Multimedia, Cyberjaya, Selangor 63100, Malaysia
[c] Sandisk Storage Malaysia Sdn. Bhd., Persiaran Cassia Selatan 1, Simpang Ampat, Pulau Pinang 14110, Malaysia
[d] Department of Chemistry, Faculty of Science, Universiti Putra Malaysia, Serdang, Selangor 43400 UPM, Malaysia

ARTICLE INFO

Keywords:
Electrochromic
Vanadium pentoxide
Sol-gel
Thin film
Optical modulation
Concentration-dependent performance

ABSTRACT

Electrochromic (EC) devices have gained significant attention in energy-saving applications, with V_2O_5 standing out owing to its excellent Li-ion intercalation and multi-color properties compared to the widely used WO_3. Nonetheless, no research has addressed the effect of V_2O_5 concentration on EC performance. Given the rising popularity of V_2O_5 in EC devices, this observation has indicated a significant research gap that should be addressed. Therefore, this study investigated the performance of V_2O_5 EC devices with concentrations ranging between 0.02 mol/L and 0.1 mol/L via sol-gel spin coating. Consequently, higher film thickness was observed as the sol-gel concentration increased, as the V_2O_5 thin films transformed from amorphous to crystalline phases. Increasing grain size with worm-like structures was also observed as the concentration increased. The EC device that balanced between optical modulation (OM), coloration efficiency (CE), and coloring (t_c) with bleaching times (t_b) was then observed for the ITO/0.08 V_2O_5/electrolyte/ITO device. This device showcased optimized values for OM (37.11 %), CE (26.53 $cm^2\ C^{-1}$), t_c (7 s), and t_b (14 s). Overall, these findings could provide novel information regarding the correlation of V_2O_5 concentration and EC device performance. A unique contribution was also presented in this study by demonstrating a direct relationship between the concentration of sol-gel precursors, the evolution of structure, and the EC performance, potentially for large-scale production and energy-efficient smart window technologies.

1. Introduction

Switchable smart glass technology has been widely explored for its potential to reduce energy consumption in many environments. The technology is also increasingly used in buildings as it can block ultraviolet (UV) and infrared (IR) light while minimizing the reliance on artificial lighting, effectively reducing heat gain and loss, protecting interiors, and offering on-demand privacy [1]. These functionalities allow smart glass to be versatile and can be integrated into homes and vehicles [2]. Therefore, research on electrochromic (EC) devices is driven by their unique ability to change optical properties with an applied voltage, leading to diverse applications including smart windows or coupled with batteries [3,4].

The common EC materials used today include TiO_2, WO_3, and V_2O_5 owing to their high coloration efficiency (CE), optical modulation (OM), versatility in preparation and application, and structural stability [5,6]. In 1930, Kobosew and Nekrassow discovered that WO_3 powders could undergo coloration by reduction in an acidic solution, making WO_3 one of the earliest documented EC technologies [7]. Nonetheless, several limitations affect the performance of EC devices. WO_3 can only exhibit a dark blue color and has limited modulation capabilities [8,9]. Likewise, V_2O_5 presents multi-color EC display capability, including orange, green, and blue, making it suitable for diverse display applications [10]. In its most stable phase, V_2O_5 undergoes reversible redox reactions

* Corresponding author at: Centre for Advanced Devices and Systems, Centre of Excellence for Robotics and Sensing Technologies, Multimedia University, Persiaran Multimedia, Cyberjaya, Selangor 63100, Malaysia
E-mail address: kychan@mmu.edu.my (K.-Y. Chan).

https://doi.org/10.1016/j.mtcomm.2026.114653
Received 24 November 2025; Received in revised form 1 January 2026; Accepted 9 January 2026
Available online 12 January 2026

involving Li-ion intercalation and deintercalation to achieve multi-color transitions [11]. These reactions alter the oxidation state of V and modify the optical features of a material, leading to different colors. The reaction is described as follows [12]:

$$V_2O_5 + xLi^+ + xe^+ \leftrightarrow Li_xV_2O_5 \quad (1)$$

The performance of these devices is crucial for their practical applications. Numerous performance metrics include OM, switching speed, CE, and stability [13,14]. These performance metrics highly depend on the fabrication process [15], such as the thickness [16], and particularly for the sol-gel method, the sol concentration. Various studies focus on material design for V_2O_5 EC devices. For example, Panagopoulou *et al.* reported that W doping in V_2O_5 enhanced CE [17]. Although increasing attention towards V_2O_5 thin films is observed, there is no work focusing on the impact of sol-gel concentration on EC device performance.

The viscosity, precursor ratio, and hydrolysis-condensation kinetics of a solution are dependent on its sol-gel concentration. In turn, the concentration determines film thickness, porosity, crystallinity, and stoichiometry after annealing. Structural and morphological features of a film can then determine the degree of ion-diffusion-limited charge storage and the OM performance in EC devices [18,19]. Thus, balanced optical contrast, CE, and cycling stability in V_2O_5-based EC systems require well-tailored sol–gel concentrations. Much research on the EC properties of the V_2O_5 also primarily focused on the thin film level under controlled conditions. This approach neglects the crucial step of investigating real-world applications of practical devices, such as the sol-gel method.

According to the authors' understanding, previous studies did not examine how V_2O_5 sol-gel concentration influenced EC performance (EC device rather than film properties). In this study, the novelty was found within the thorough examination of sol-gel precursor concentration as a crucial processing factor, alongside demonstrating its direct relationship with structural development and EC performance (OM, ion diffusion behavior, and switching kinetics). From an application perspective, scalable fabrication and optimization of V_2O_5-based EC devices could also be accomplished for smart window and energy-efficient building applications [20,21].

This study fabricated V_2O_5 thin films (0.02–0.10 mol/L) using the sol-gel spin coating approach and assembled them into EC devices using lithium perchlorate ($LiClO_4$) as the electrolyte. The device structure selected in this study was indium tin oxide (ITO)/V_2O_5/electrolyte/ITO. The devices then underwent X-ray diffraction (XRD), field-emission scanning electron microscopy (FESEM), cyclic voltammetry (CV), chronoamperometry (CA), energy-dispersive X-ray spectroscopy (EDX), and UV-Vis spectroscopy to investigate their performance based on structural and optical characteristics. Collectively, this study demonstrated an approach to optimize the performance of V2O5-based EC devices via sol-gel spin coating.

2. Materials and methods

2.1. Materials

This work acquired several chemicals from Sigma-Aldrich, Rockville, MD, USA, including acetonitrile (ACN), 30 % hydrogen peroxide (H_2O_2), V_2O_5 powder, $LiClO_4$, propylene carbonate (PC), and polymethylmethacrylate (PMMA). All chemicals were utilized as acquired, without needing additional purification.

2.2. Synthesis of the V_2O_5 Sol-Gels

Fig. 1 depicts the step-by-step process of the sol-gel fabrication for V_2O_5. This sol-gel preparation involved adding 15 ml of H_2O_2 (30 %) to deionized water (15 ml). The mixture was stirred for 10 mins at ambient temperature prior to adding 0.5456 g of V_2O_5 powder. This mixture was immediately stirred at 70°C for 6 mins, and the exothermic reaction occurred. The mixture was then stirred for another 3 mins, in which a dark red solution was obtained. Subsequently, four separate solutions were prepared by diluting 4 ml, 3 ml, 2 ml, and 1 ml of the solutions with 1 ml, 2 ml, 3 ml, and 4 ml of DI water to obtain 0.08 mol/L, 0.06 mol/L, 0.04 mol/L, and 0.02 mol/L solutions, respectively. The sol-gels were finally kept in their respective glass vials and aged for at least 48 h.

2.3. Preparation of the ITO/V_2O_5/electrolyte/ITO EC devices

The sol-gel was spin-coated using indium tin oxide (ITO) substrates based on sol-gel spin coating at 3000 rpm. This process was repeated five times on an active area of 2.4 cm^2 to achieve five layers of V_2O_5. The films were then immediately annealed at 200°C (1 h). Subsequently, the V_2O_5-based EC device was assembled and sealed with UV resin to contain the gel electrolyte. This study fabricated the Li^+ gel electrolyte following the methodology adapted from our previous work [22]. In brief, the electrolyte was prepared by combining PC [50 % v/v (12.5 ml)], $LiClO_4$ [1 M (2.6598 g)], and PMMA [28 % w/v (7 g)] in a 25 ml ACN solution. This mixture was stirred at a medium speed for 24 h. The mixture was then baked at 90°C for 1 h to produce a highly viscous gel-like solution. Lastly, the V_2O_5-based EC devices prepared in this study contained 0.02 mol/L, 0.04 mol/L, 0.06 mol/L, 0.08 mol/L, 0.10 mol/L of V_2O_5: (i) ITO/0.02 V_2O_5/electrolyte/ITO, (ii) ITO/0.04 V_2O_5/electrolyte/ITO, (iii) ITO/0.06 V_2O_5/electrolyte/ITO, (iv) ITO/0.08 V_2O_5/electrolyte/ITO, and (v) ITO/0.10 V_2O_5/electrolyte/ITO.

2.4. Characterization tools

The analysis concerning the V_2O_5 thin films was carried out via an XRD instrument (Shimadzu) employing Cu Kα radiation (λ = 1.540598 Å), with measurements taken across a 2θ range of 20° to 60°. Surface morphology and cross-sectional views were also assessed via a

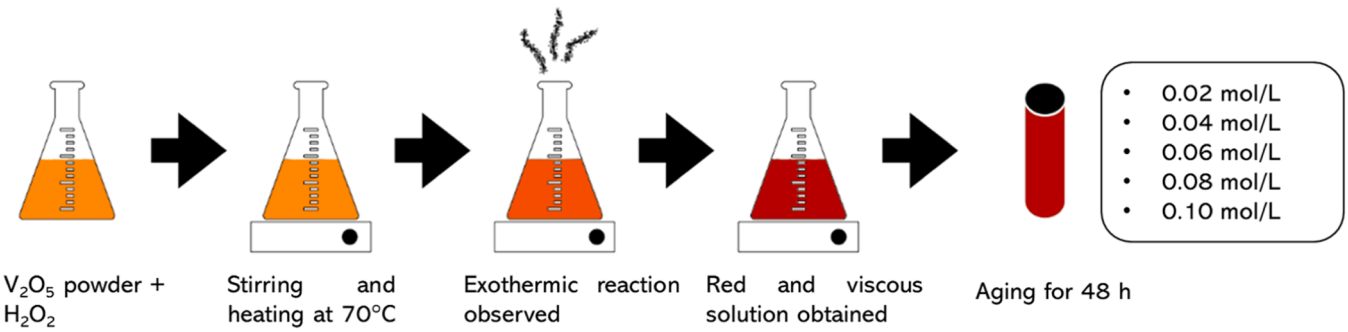

Fig. 1. The fabrication process of the V_2O_5 sol-gels (0.02–0.10 mol/L).

FESEM tool (Nova NanoSEM 450). Meanwhile, elemental composition was assessed using an EDX spectrometer (Oxford Instruments). Optical transmittance measurements were then taken with the UV-Vis spectrophotometer (Avantes AvaSpec-2048L). Finally, the EC properties regarding the V_2O_5-based EC devices containing between 0.02 mol/L and 0.10 mol/L of V_2O_5 were evaluated using CA and CV techniques (Autolab PGSTAT204).

3. Results and Discussion

3.1. Structural properties of V_2O_5 thin films

Fig. 2 portrays the XRD outcomes of V_2O_5 films deposited at 0.02 mol/L to 0.10 mol/L. Only diffraction peaks representing the (222) and (400) planes of the ITO substrate were observed at 30.2° and 35.2° for the 0.02 mol/L and 0.04 mol/L V_2O_5 thin films (ICDD no. 06–0416) [23]. The characteristic diffraction peaks of V_2O_5 were also not present, suggesting that the films were amorphous. Nevertheless, weak peaks denoting the (110) plane of orthorhombic V_2O_5 were observed at 24.7° for the 0.06 mol/L V_2O_5 film, indicating some crystalline nature. This (110) plane of orthorhombic V_2O_5 then grew more intense with rising concentration from 0.06 mol/L to 0.10 mol/L, while weak (011) and (002) planes of orthorhombic V_2O_5 were observed for the 0.08 mol/L and 0.10 mol/L V_2O_5 thin films (ICDD no. 01–089–0612) [24,25]. Interestingly, there was a strong and sharp peak representing the (001) plane of orthorhombic V_2O_5 at 20.3° for the 0.10 mol/L V_2O_5 film. This peak was not present for V_2O_5 thin films deposited at other concentrations, implying a high crystallinity for the 0.10 mol/L V_2O_5 film.

This increasing trend of characteristic peak intensities could be understood by measuring the grain size (D_g) of the V_2O_5. The values can be computed using Scherrer's formula, which is provided as follows [26]:

$$D_g = (0.9\lambda)/(\mathrm{FWHM} \times cos\theta) \quad (2)$$

where λ denotes the X-ray wavelength; FWHM denotes the full width at half maximum of the diffraction peak; and θ denotes the half of the diffraction angle (Bragg angle). Table 1 tabulates the average D_g of the various samples calculated using the (110) plane, in which there are no peaks observed for the 0.02 and 0.04 mol/L V_2O_5 films. Therefore, their average D_g could not be calculated. For the other films, there was a corresponding rise in the number of available nuclei and the density of the deposited layers with a larger precursor solution content in the sol-gel process. This process seemed to promote more effective atomic rearrangement during the annealing process, leading to improved crystal growth [27,28]. Thus, the increasing trend of D_g observed for 0.06 mol/L, 0.08 mol/L, and 0.10 mol/L V_2O_5 films was validated.

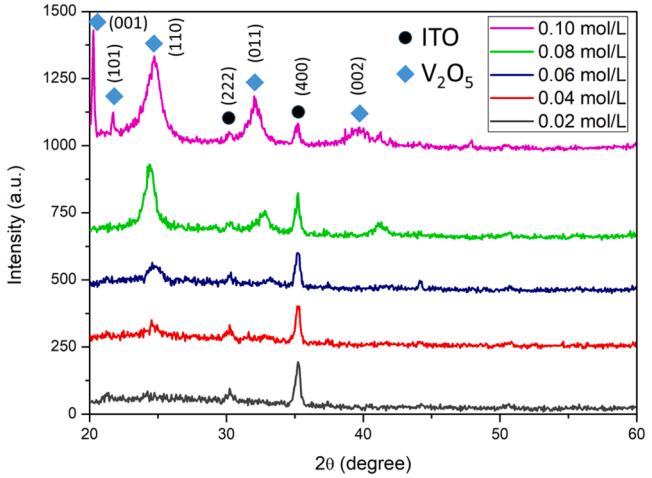

Fig. 2. The XRD spectra of V_2O_5 films deposited at 0.02 mol/L to 0.10 mol/L.

Table 1
Summary of the average D_g values obtained for the V_2O_5 films deposited at 0.02 mol/L to 0.10 mol/L.

Concentration (mol/L)	D_g (nm)
0.02	-[a]
0.04	-[a]
0.06	13.6
0.08	18.1
0.10	67.3

[a] No peaks observed for the (110) plane.

Fig. 3 portrays the cross-sectional FESEM images concerning V_2O_5 films fabricated from 0.02 mol/L to 0.10 mol/L. The images implied that as higher sol-gel concentrations were used, film thickness was higher, which was consistent with findings in the literature on thin films synthesized based on the sol-gel approach [29]. Notable increase in thickness was also observed, rising from 291 nm to 699 nm with rising concentration (0.08–0.10 mol/L). Specifically, the thickness obtained in this study aligned closely with those documented in existing literature for V_2O_5 films produced at comparable concentrations, affirming the reliability of the current findings [22]. The optical properties section below presents a more detailed discussion on the relationship between thickness and optical transmittance, noting that a similar trend of decreasing transmittance has been observed in other studies [22,30].

It could be observed that with an increase in precursor concentration, the V_2O_5 film produced at 0.06 mol/L was somewhat thinner than that at 0.04 mol/L. Both dynamics of spin-coating, alongside the structural changes that occurred during post-annealing, were probably the cause of this effect [31]. As previously mentioned in the XRD analysis, the 0.04 mol/L film was predominantly amorphous, while improved crystallinity was then recorded for the 0.04 mol/L film (see Fig. 2). This higher crystallinity could be ascribed to the greater extent of network condensation and densification processes occurring during annealing. Certain sol-gel-related studies also reported that as the amorphous network transitioned into a more compact crystalline arrangement, a decrease in film volume perpendicular to the substrate could occur from both processes [32–34]. As such, even when the precursor molarity was higher, a thinner final film at intermediate concentrations was obtained during spin coating owing to densification (amorphous → crystalline).

Fig. 4 portrays the top-view FESEM images of the V_2O_5 films fabricated at 0.02 mol/L to 0.10 mol/L. The morphological properties of the films were characterized by FESEM at 50,000 times magnification using a through-lens detector, alongside a 10.00 kV accelerating voltage (working distance = 5.2 mm). Rather than changes in imaging parameters, differences in surface appearance arose from intrinsic morphological variations among the films. At 0.02 mol/L, the V_2O_5 film appeared to have a relatively uniform morphology with fine-grained structure. As the concentration increased (0.04 mol/L), the texture on the surface became more pronounced. Surprisingly, worm-like structures began to form at 0.06 mol/L. At 0.10 mol/L, the diameter grew to around 10 times the previous size. This outcome could be explained by the increase in the electrostatic forces between solute particles as the solute concentration rose, causing the formation of larger grains [29]. Table 2 then lists the average diameter (D_a) of the worm-like structures observed on the thin films.

3.2. Elemental composition of V_2O_5 thin films

Fig. 5 depicts the elemental composition of the V_2O_5 films at 0.02 mol/L to 0.10 mol/L determined by EDX. The EDX spectra confirmed the expected elements of V, O, In, and Sn. At lower concentrations (0.02–0.06 mol/L), stronger In and Sn peaks were observed due to thinner V_2O_5 films. Thicker films then suppressed substrate signals at higher concentrations (0.08–0.10 mol/L), emphasizing V and O.

Table 3 lists the atomic percentage of V_2O_5 films prepared at

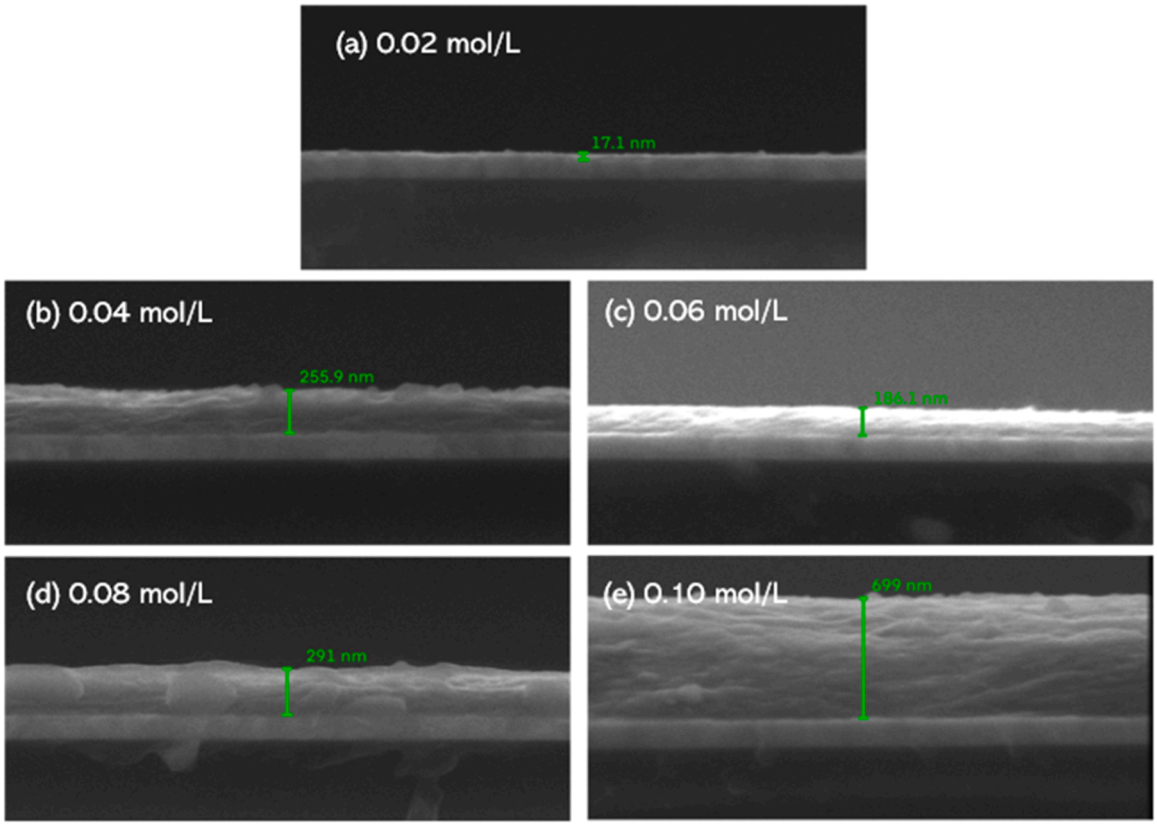

Fig. 3. The cross-section FESEM images reveal the thickness of V_2O_5 thin films at (a) 0.02 mol/L, (b) 0.04 mol/L, (c) 0.06 mol/L, (d) 0.08 mol/L, and (e) 0.10 mol/L.

different concentrations. As concentration increased, the atomic percentage of V increased while O decreased. This trend occurred because the increasing thickness reduced the O signal from the substrate. With the rising film thickness, the detection of the substrate's O signal diminished while the measurement of the film's V intensified, changing the atomic percentage [35]. This observation could also be attributed to kinetically limited oxidation caused by rapid deposition [36]. When the film was deposited at an accelerated rate, oxygen might not have sufficient time to diffuse throughout all areas, leading to incomplete oxidation and an elevated V-to-O ratio.

For the atomic ratios of V_2O_5 0.08 mol/L and 0.10 mol/L samples, the observed discrepancies could be attributed to the EDX quantification limitations for oxides [37]. Rather than indicating the existence of a secondary phase, diminished sensitivity for lighter elements (including oxygen) might occur for EDX as a semi-quantitative method due to several reasons, such as low X-ray counts and differential absorption [38,39]. Particularly, no additional crystalline phases present beyond orthorhombic V_2O_5 were demonstrated from the XRD results (see Fig. 2). Hence, the films were inferred to maintain phase purity, and any observed deviations in stoichiometry were likely due to measurement deviations.

3.3. Optical characteristics of V_2O_5 thin films

Fig. 6 presents the virgin film transmittance spectra of V_2O_5 films deposited at 0.02 mol/L to 0.10 mol/L. Increased sol-gel concentration corresponded to larger particle size and an elevated defect or impurity state density. These alterations diminished quantum confinement and generated mid-gap states. Therefore, the edge of the transmittance curve shifted towards longer wavelengths, indicating a reduced effective bandgap [40]. Also, there was a greater decrease in transmittance at longer wavelengths as precursor concentration was increased. This outcome might be due to greater concentration, which increased surface roughness and D_g, leading to greater light scattering. Accordingly, transmittance was reduced more within the longer wavelength region. This type of transmittance and thickness dependence was also observed in V_2O_5 films, which, when thickened, continuously led to a transmittance drop in all wavelength regions [41].

As V_2O_5 concentration increased, the observed red shift within the absorption edge was qualitatively linked to the defect-related states within the bandgap. In transition-metal oxides processed through sol-gel methods, the presence of structural disorder, oxygen vacancies, and mixed valence states (V^{4+}/V^{5+}) was recognised to create localised mid-gap states. Hence, towards lower photon energies, the broadening of the absorption tail could be observed. Typically, defect-induced band tailing appears as a red shift within the absorption edge, accompanied by increased sub-bandgap absorption [12,42]. Although this study did not include a quantitative Urbach energy or Tauc analysis, the optical behaviour observed aligned with defect-assisted absorption mechanisms that were extensively documented for sol-gel-derived V_2O_5 and other oxide EC films [43–45].

3.4. EC properties of the ITO/V_2O_5/electrolyte/ITO EC devices

Fig. 7 presents the CV and diffusion coefficient (D_c) graphs of the ITO/V_2O_5/electrolyte/ITO EC devices for different V_2O_5 concentrations. The CV measurements were performed between −2 V and 2.5 V (scan rate = 0.1 V/s). These CV curves showed cathodic and anodic peaks, indicating that the reaction was a reversible redox process involving charge insertion and extraction. With larger V_2O_5 concentrations from 0.02 mol/L to 0.10 mol/L, the cathodic peak current (i_p) rose from −0.49 mA to −1.83 mA (see Table 4). This finding demonstrated that the increasing concentration of V_2O_5 contributed to the number of charge insertions.

The results obtained from the CV measurements are employed to compute the D_c for the Li^+ ions based on the Randles-Sevcik equation as

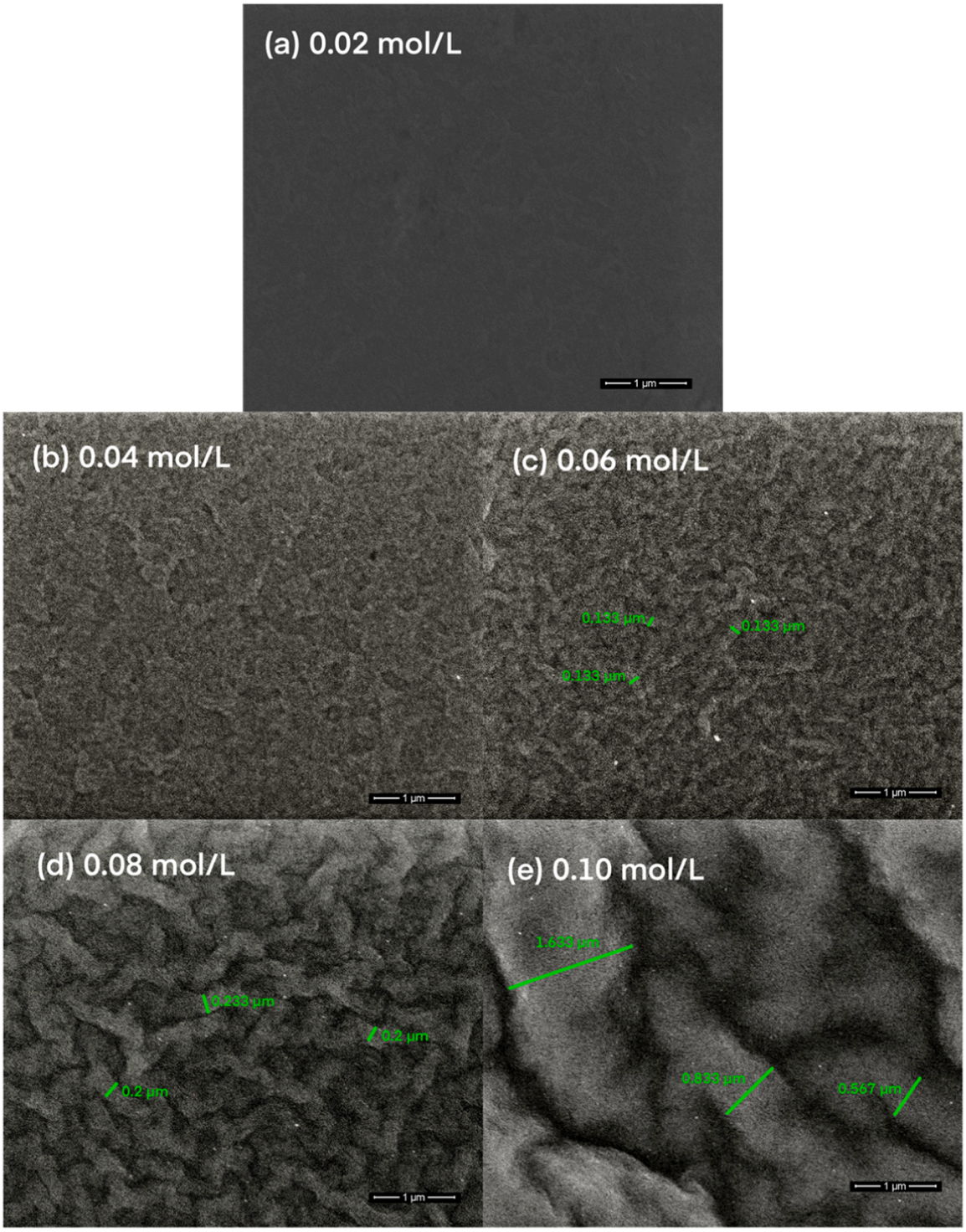

Fig. 4. The top-view FESEM images of V_2O_5 films fabricated at (a) 0.02 mol/L, (b) 0.04 mol/L, (c) 0.06 mol/L, (d) 0.08 mol/L, and (e) 0.10 mol/L. Selected D_a measurements are presented in these images.

follows [46]:

$$i_p = 2.69 \times 10^5 \times A \times n^{\frac{3}{2}} \times D_c^{\frac{1}{2}} \times C_o \times v^{\frac{1}{2}} \quad (3)$$

where n represents the number of electrons transferred within the redox reaction (1); C_o represents the electrolyte concentration; A represents the electrode surface area; and v represents the scan rate. Fig. 7**(c)** also provides a schematic representation of the EC mechanism within the ITO/ V_2O_5/electrolyte/ITO device. This mechanism involved the reversible insertion and extraction of Li^+ ions, which was coupled with the V^{5+}/V^{4+} redox mechanism, leading to the cathodic and anodic characteristics evident in the CV curves.

The ITO/0.10 V_2O_5/electrolyte/ITO device demonstrated the highest D_c of 7.86×10^{-17} cm^2 s^{-1}. This observation was due to the more porous film structure at higher concentration, providing a shorter diffusion path length that allowed ions to move quickly into the EC layer [47,48]. Meanwhile, the ITO/0.02 V_2O_5/electrolyte/ITO device showed the lowest D_c of 0.56×10^{-17} cm^2 s^{-1}. This observation could be

Table 2
Summary of the D_a values of the worm-like structures on V_2O_5 thin films deposited at various concentrations at 0.02 mol/L to 0.10 mol/L.

Concentration (mol/L)	D_a (μm)
0.02	-[a]
0.04	-[a]
0.06	0.134 ± 0.004
0.08	0.211 ± 0.019
0.10	0.943 ± 0.273

[a] D_a cannot be calculated due to the FESEM tool's capability at maximum magnification.

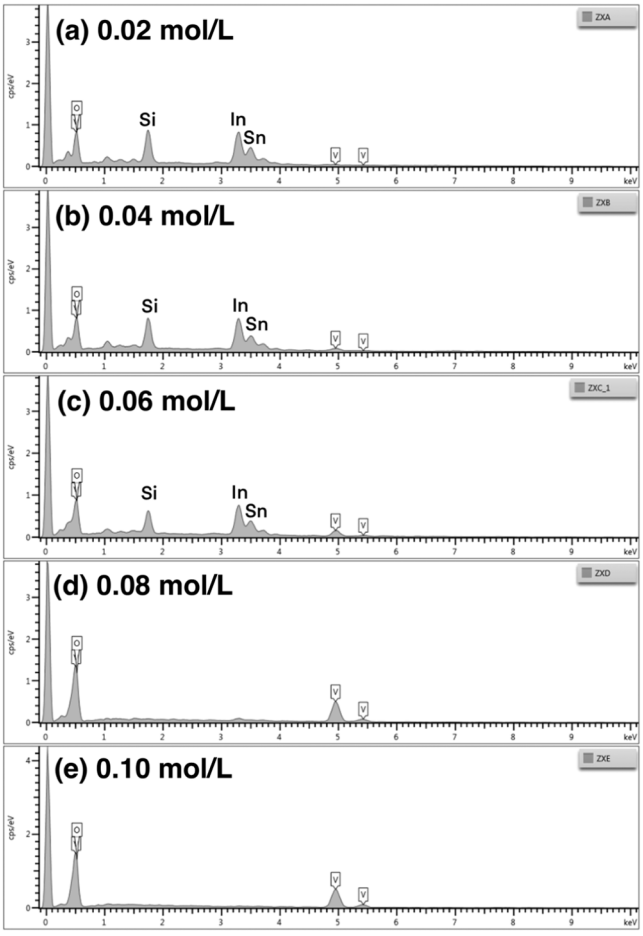

Fig. 5. The EDX results of V_2O_5 films fabricated at (a) 0.02 mol/L, (b) 0.04 mol/L, (c) 0.06 mol/L, (d) 0.08 mol/L, and (e) 0.10 mol/L.

Table 3
Summary of the elemental composition of V_2O_5 films deposited at 0.02 mol/L to 0.10 mol/L.

Concentration (mol/L)	Atomic Ratio (%)	
	V	O
0.02	5.36	94.64
0.04	17.39	82.61
0.06	34.88	65.12
0.08	70.86	29.14
0.10	70.19	29.81

attributed to the less porous film structure at lower concentration, having a longer diffusion path length for more ions to move into the EC layer. The D_c values obtained by all the ITO/ V_2O_5/electrolyte/ITO devices were also consistent with devices fabricated using the sol-gel method [47,49]. Notably, a higher D_c as concentration increased indicated a faster kinetic response and revealed a higher ion diffusivity. The more extensive layer under the CV graph also showed the larger charge capacity of the EC devices as concentration increased [30].

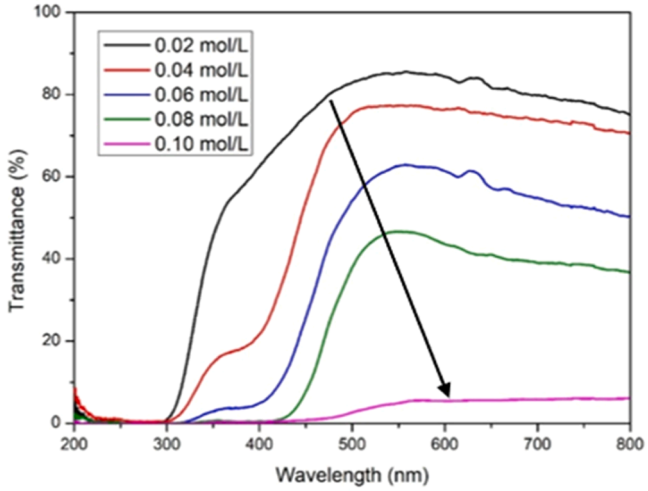

Fig. 6. The virgin transmittance spectra of the V_2O_5 thin films at 0.02 mol/L to 0.10 mol/L.

Fig. 8 depicts the CA measurements of the ITO/V_2O_5/electrolyte/ITO EC devices for different V_2O_5 concentrations (step potential = −2 V–2.5 V, 60 s). Following this process, UV–vis spectroscopy was utilized to assess the transmittance of the V_2O_5 EC devices (wavelength = 633 nm). This data demonstrated the OM capability (ΔT), which can be computed in this study as follows:

$$\Delta T(\%) = T_b(\%) - T_c(\%) \quad (4)$$

where T_c and T_b denote the bleaching and coloring transmittances, respectively.

Fig. 8**(f)** illustrates that as the concentration increases, the OM elevates but reaches saturation at 0.08 mol/L. At this point, the OM then decreased for the ITO/0.10 V_2O_5/electrolyte/ITO device. This trend was likely attributed to the thickness effect, which increased with sol-gel concentration as confirmed by the FESEM images [22,30]. Notably, the drop in OM was ascribed to the rough surface and higher D_g of the V_2O_5 film fabricated at a larger concentration, which impeded ion diffusion [50]. The D_g was also the highest for the 0.10 mol/L V_2O_5 films, revealing large worm-like structures. Likewise, the decrease in overall transmittance likely contributed to the suppression in OM, which was reported by other researchers [49,50].

Table 5 compares the difference between T_c and T_b of the ITO/V_2O_5/electrolyte/ITO EC devices at various concentrations. The results denoted that T_c and T_b decreased with rising concentration, owing to the higher light scattering properties of the thin film as surface roughness increased (higher concentration) [51,52]. The ITO/0.08 V_2O_5/electrolyte/ITO EC device also exhibited the highest OM of 37.11 %. Nevertheless, this value declined for ITO/0.10 V_2O_5/electrolyte/ITO (19.18 %), which might be caused by ion-trapping when Li ions were injected into the film at high concentrations [53].

When comparing the FESEM cross-sections (170–699 nm), correlations were observed between thickness, optical transmittance, and ΔT. For EC oxides, greater optical absorption and optical density (OD) could be accomplished when the films became thicker, alongside a change from amorphous to crystalline structure [45]. Nevertheless, when exceeding an optimal range, bleached-state transmittance and OM might reduce due to increased baseline absorption or scattering (even though charge storage could improve) [54]. Thus, when the concentration was

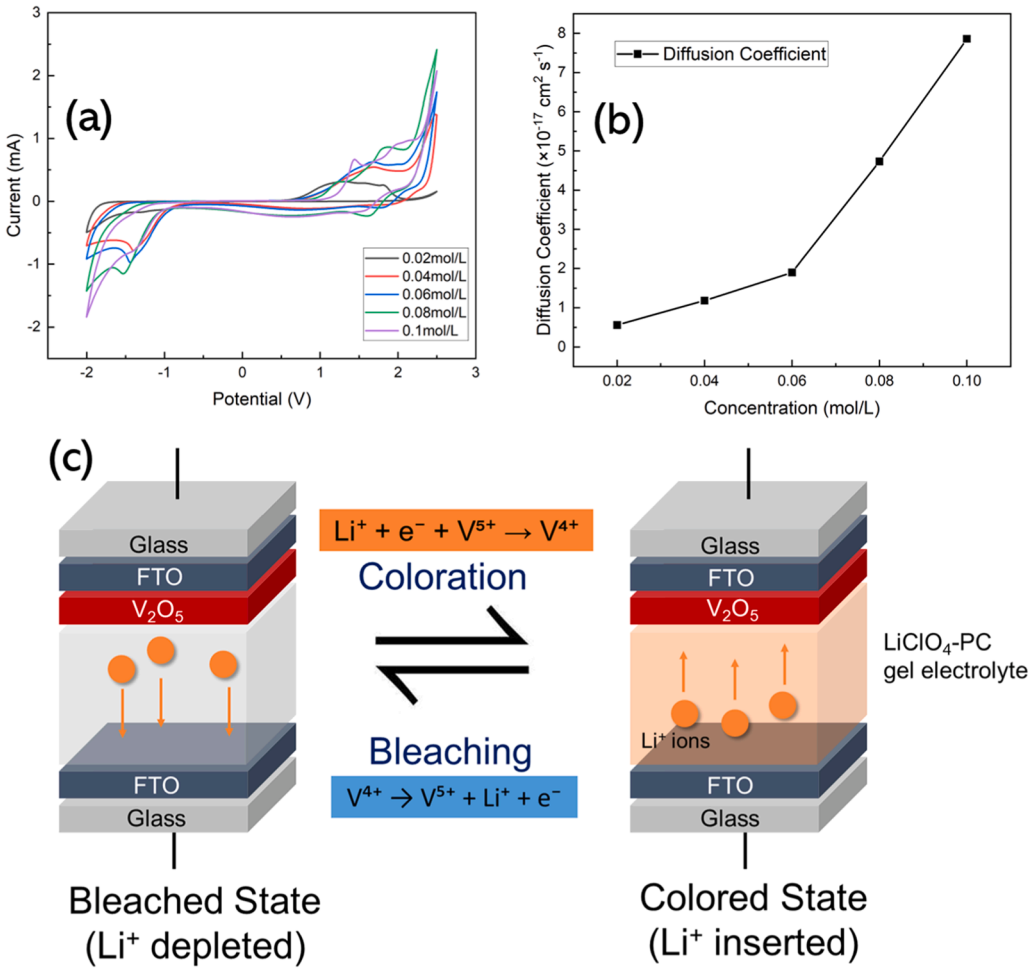

Fig. 7. (a) The CV graphs and (d) D_g values of the ITO/V_2O_5/electrolyte/ITO EC devices fabricated at various sol concentrations. (c) Schematic of Li^+ intercalation/deintercalation and the corresponding V^{5+}/V^{4+} redox mechanism governing coloration and bleaching.

Table 4
Summary of the D_c values obtained for the ITO/V_2O_5/electrolyte/ITO EC devices at 0.02 mol/L to 0.10 mol/L.

Device	i_p (mA)	D_c ($\times 10^{-17}$ cm^2 s^{-1})
ITO/0.02 V_2O_5/electrolyte/ITO	-0.49	0.56
ITO/0.04 V_2O_5/electrolyte/ITO	-0.71	1.18
ITO/0.06 V_2O_5/electrolyte/ITO	-0.90	1.90
ITO/0.08 V_2O_5/electrolyte/ITO	-1.42	4.73
ITO/0.10 V_2O_5/electrolyte/ITO	-1.83	7.86

further increased to 0.10 mol/L, ΔT decreased to 19.18 %, despite continued film thickening. Previous studies also documented the trade-off between thickness and optical properties for WO_3 films, indicating that the modulation of transmittance was significantly influenced by thickness [54,55]. As such, maximising ΔT could be attained at an optimal intermediate thickness.

Generally, CE is a critical variable in the performance of EC devices. This parameter is a measure of how effectively the EC device can undergo color change with the intercalation of an electric charge and is denoted as the change in OD per unit charge density (Q_A), which is computed as follows [56]:

$$CE = \frac{\Delta(OD)}{Q_A} = \frac{\log\left(\frac{T_b}{T_c}\right)}{Q_A} \quad (5)$$

where Q_A represents the intercalated charge per unit area. Fig. 9**(a)** then illustrates that the CE saturates at around 0.06 mol/L, which is attributed to high OM. Fig. 9**(b)** also displays the correlation between OD and Q_A.

Within an EC device, increasing the inserted charge increased the number of sites switched, which in turn elevated OD, but only to the extent that most of the film was modulated. Beyond this, modulated charge produced increasingly fewer returns, which was the reason for the increase in the CE. These CE and charge characteristics were also observed in other metal oxide-related studies, supporting this observation [57]. In contrast, it was apparent from the CE that declining above 0.06 mol/L was highly likely because the thicker films reduced the fraction of inserted charge that actually switched active sites, lowering the optical change per unit charge [58].

Fig. 10 illustrates the coloring (t_c) and bleaching times (t_b) of the ITO/V_2O_5/electrolyte/ITO EC devices at various concentrations, revealing that as the sol-gel concentration increases, the t_c and t_b rise. This trend was similar to that observed for switching time, crystallinity, and film thickness, suggesting a correlation among these properties. Table 6 then compiles all data regarding t_c, t_b, OD, and CE of these ITO/V_2O_5/electrolyte/ITO EC devices. Results indicated that the CE increased with concentration and saturated at 27.9 cm^2 C^{-1} for the ITO/0.06 V_2O_5/electrolyte/ITO device. This observation could be attributed to surface cracks due to increased agglomeration and faster evaporation rates during the sol-gel annealing process [59].

The observation revealed a significant increase in switching time from ITO/0.08 V_2O_5/electrolyte/ITO to ITO/0.10 V_2O_5/electrolyte/ITO devices, which was demonstrated by the rise in t_c and t_b of 7 s to 18 s and

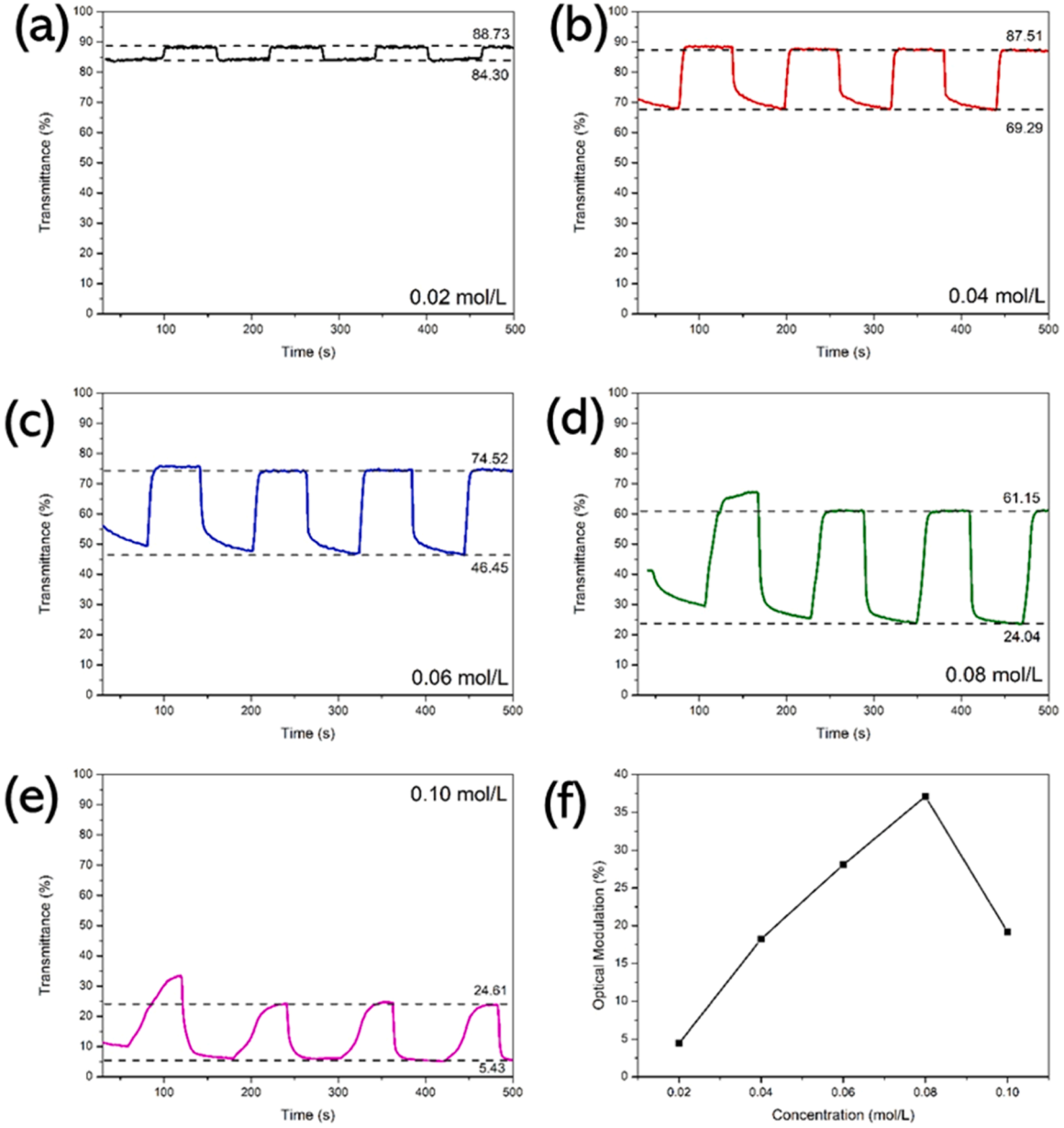

Fig. 8. (a) The transmittance responses of the (a) ITO/0.02 V_2O_5/electrolyte/ITO, (b) ITO/0.04 V_2O_5/electrolyte/ITO, (c) ITO/0.06 V_2O_5/electrolyte/ITO, (d) ITO/0.08 V_2O_5/electrolyte/ITO, and (e) ITO/0.10 V_2O_5/electrolyte/ITO EC devices. (f) The OM values of the ITO/V_2O_5/electrolyte/ITO EC devices at various concentrations.

Table 5
Summary of the coloring and bleaching transmittances of the ITO/V_2O_5/electrolyte/ITO EC devices 0.02 mol/L to 0.10 mol/L.

Device	T_c (%)	T_b (%)	ΔT (%)
ITO/0.02 V_2O_5/electrolyte/ITO	84.30	88.73	4.43
ITO/0.04 V_2O_5/electrolyte/ITO	69.29	87.51	18.22
ITO/0.06 V_2O_5/electrolyte/ITO	46.45	74.52	28.07
ITO/0.08 V_2O_5/electrolyte/ITO	24.04	61.15	37.11
ITO/0.10 V_2O_5/electrolyte/ITO	5.43	24.61	19.18

14 s to 31.9 s, respectively. This finding was ascribed to the higher crystallinity and roughness at higher concentrations, hindering ion insertion and extraction [47,48]. The result was probably due to the higher sol concentration, which gave rise to a thicker, more crystalline film, increasing the pathways for ion insertion or extraction and slowing the kinetics.

In earlier studies, slower Li^+ diffusion kinetics were reported with high crystallinity V_2O_5 films containing denser packing and lower defect density. Hence, the effective diffusion path length was extended, alongside restricting the number of ion intercalation sites. This process could then lead to longer durations for both colouring and bleaching processes, as observed with ITO/0.10 V_2O_5/electrolyte/ITO [60,61]. Conversely, the ITO/0.02 V_2O_5/electrolyte/ITO and ITO/0.04 V_2O_5/electrolyte/ITO had the lowest t_c and t_b of 6.2 s or 1.2 s and 1.23 s or 4 s, respectively. This observation could be attributed to a more amorphous structure at lower concentrations, facilitating faster ion insertion and removal [48].

From the CV measurements, D_c represented the local ionic mobility present within the V_2O_5 films when subjected to minor perturbations (see Fig. 7). Nevertheless, the overall switching kinetics at the device level were indicated by t_c and t_b values (see Fig. 10), which could be further affected by various factors [62,63]. Such examples of these factors entailed thickness, crystallinity, and the distance of ion

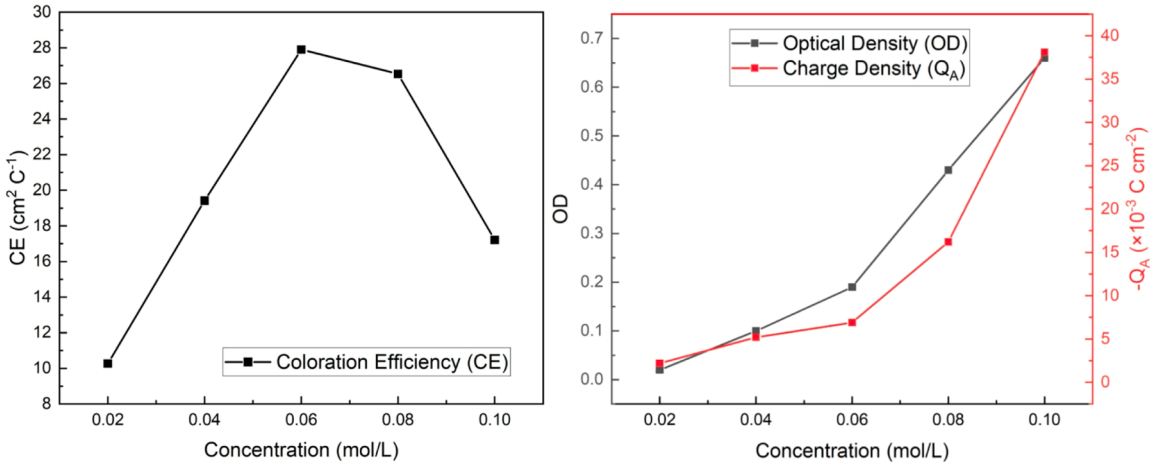

Fig. 9. (a) The CE and (b) optical and charge density of the ITO/V_2O_5/electrolyte/ITO EC devices at 0.02 mol/L to 0.10 mol/L.

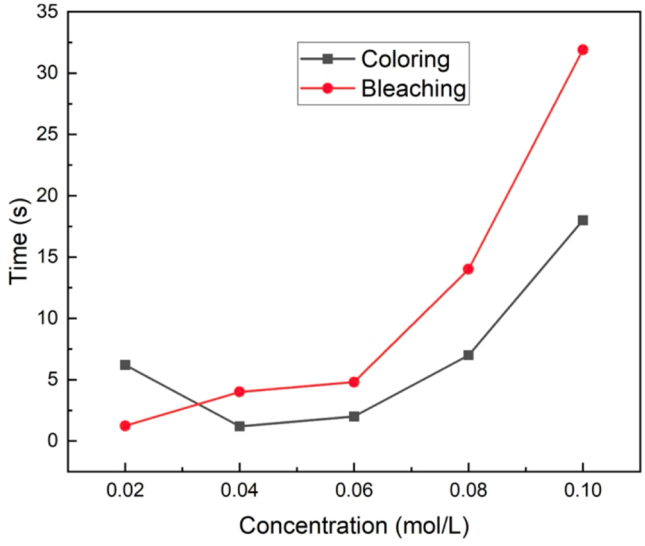

Fig. 10. The t_c and t_b values of ITO/V_2O_5/electrolyte/ITO EC devices at 0.02 mol/L to 0.10 mol/L.

Table 6
Summary of the coloring and bleaching kinetics of ITO/V_2O_5/electrolyte/ITO EC devices at 0.02 mol/L to 0.10 mol/L.

Device	t_c (s)	t_b (s)	ΔOD	Q_A (× 10^{-3} C cm^{-2})	CE (cm^2 C^{-1})
ITO/0.02 V_2O_5/ electrolyte/ITO	6.2	1.23	0.0222	2.2	10.27
ITO/0.04 V_2O_5/ electrolyte/ITO	1.2	4	0.101	5.2	19.42
ITO/0.06 V_2O_5/ electrolyte/ITO	2	4.8	0.192	6.9	27.9
ITO/0.08 V_2O_5/ electrolyte/ITO	7	14	0.43	16.2	26.53
ITO/0.10 V_2O_5/ electrolyte/ITO	18	31.9	0.656	38.1	17.21

transport. As such, films that were thicker and more crystalline might demonstrate extended switching times. This outcome could be attributed to the longer diffusion path lengths and interfacial resistance [60].

In order to substantiate the choice of 0.08 mol/L as the most effective concentration, a multi-parameter spider plot is illustrated in Fig. 11. All parameters (OM, CE, t_c, t_b, OD, and Q_A) were normalized to facilitate

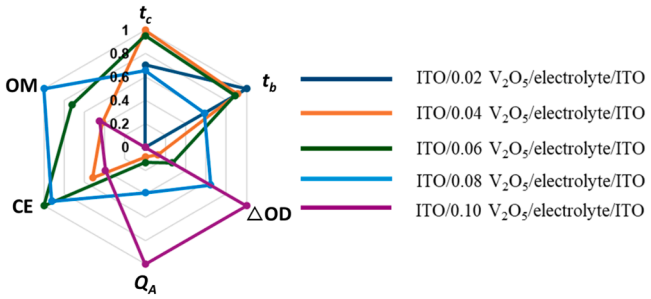

Fig. 11. The spider plot comparing EC performance parameters of ITO/V_2O_5/electrolyte/ITO EC devices at 0.02 mol/L to 0.10 mol/L concerning OM, OD, CE, t_c, t_b, and Q_A. The t_c and t_b values are inversely normalized so that larger radial values represent improved performance. All parameters are also scaled to the range 0–1 using min-max normalization.

direct comparison. Although ITO/0.10 V_2O_5/electrolyte/ITO demonstrated larger Q_A and OD, it revealed a relative increase in switching times, alongside small CE. Therefore, at higher concentrations, the increased film thickness could compromise overall EC performance [62]. Conversely, ITO/0.80 V_2O_5/electrolyte/ITO exhibited the most balanced performance among all parameters, strengthening its classification as the best concentration.

Overall, comparing all devices revealed that the ITO/0.08 V_2O_5/electrolyte/ITO device possessed the most optimal potential. This conclusion was based on the optimized values for OM (37.11 %), CE (26.53 cm^2 C^{-1}), OD (0.43), t_c (7 s), and t_b (14 s) observed in this device. Nonetheless, further analysis was still required to validate these outcomes. Several limitations still need to be addressed to understand the potential of V_2O_5-based devices, including the limited range of sol concentrations, long-term stability analysis, and in-depth oxidation state analysis.

From these observations, ITO/0.08 V_2O_5/electrolyte/ITO was selected for the stability measurements. In Fig. 12, the temporal transmittance response of ITO/0.08 V_2O_5/electrolyte/ITO is depicted. During periodic switching, the stability measurements were conducted over 6000 s (50 coloration-bleaching cycles, 120 s each cycle). Initially, the device demonstrated significant initial EC activity, achieving an OM = ~30 % (~16 cycles). Nonetheless, ongoing cycling then led to a gradual decrease in OM, suggesting a constrained level of cycling stability. This degradation could be linked to ion trapping and structural fatigue resulting from the repeated intercalation and deintercalation of Li^+ within the V_2O_5 lattice.

Even though extended endurance testing is frequently documented

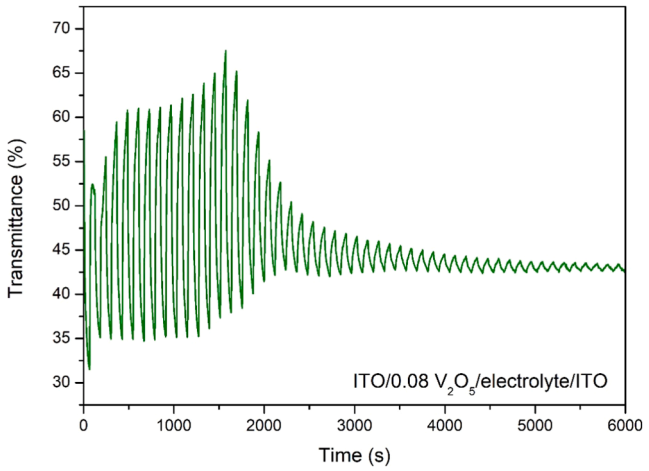

Fig. 12. The stability for ITO/0.08 V_2O_5/electrolyte/ITO, indicating coloring and bleaching transmittances utilising CA.

for highly stable EC systems (WO_3) [64], this study emphasized the intrinsic cycling behavior of pure V_2O_5 films. Fig. 12 illustrates that the device demonstrates significant degradation during the initial 50 cycles, a behavior typical of undoped V_2O_5, as extensively documented in existing studies [45,65]. Thus, the observed instability underscored the importance of employing material engineering strategies. For instance, the incorporation of dopants (Ti) enhanced the structural integrity of V_2O_5, alongside mitigating degradation throughout the cycling process [66]. Another study introduced controlled vacancy defects to enhance both the EC performance and stability of materials [67]. In a separate work, combining V_2O_5 with WO_3, which utilized the strong lattice framework of WO_3, could optimize ion insertion pathways [68].

In this study, the EC performance was significantly associated with the V^{4+}/V^{5+} redox couple. Nonetheless, X-ray photoelectron spectroscopy (XPS) measurements were not carried out because of limitations related to the instrumentation access. Rather, the examination of changes in oxidation states relies on indirect evidence derived from electrochemical behaviour, OM, and structural evolution. This study then proposed that future studies should further improve the V_2O_5-based EC devices in terms of repeatability, stability, and reproducibility, alongside XPS analysis.

3.5. Comparison of ITO/V_2O_5/electrolyte/ITO EC devices with literature

In Table 7, a comparison of EC performance of the optimised ITO/0.08 V_2O_5/electrolyte/ITO device, alongside representative V_2O_5- and WO_3-based systems, is demonstrated, which are documented in recent literature. Although doped and composite systems demonstrated elevated CE values, the device discussed in this study showcased competitive performance among undoped V_2O_5 films, all while preserving a balanced approach to OM and switching kinetics. As such, this comparison underscored the efficacy of optimising concentration without altering the composition. It should also be noted that in this study, the impact of sol-gel precursor concentration using undoped V_2O_5 was focused, rather than on maximizing absolute performance through compositional modification or complex architectures.

4. Conclusions

This study successfully investigated the effects of V_2O_5 concentration (0.02 mol/L to 0.10 mol/L) on the performance of EC devices. Unlike previous research that primarily examined V_2O_5 thin films, the analysis in this experiment was extended to fully assembled EC devices. By comparing the series of devices, the EC device that balanced between OM, CE, and switching time was observed for the ITO/0.08 V_2O_5/electrolyte/ITO device. The findings could then provide valuable information for improving V_2O_5-based EC device performance in future applications. Future studies should involve further analyzing these devices through in-depth tests related to V^{4+}/V^{5+} redox couple reactions, alongside improving the stability.

Table 7
Comparison summary of various EC parameters for representative V_2O_5- and WO_3-based EC devices reported in selected studies.

Material/Device	CE ($cm^2 C^{-1}$)	OM/ΔT (%)	t_c/t_b (s)	Reference
V_2O_5 (annealed 200 °C)	34.93	42.32	0.4/3	[69]
V_2O_5 with oxygen-vacancy nanosheets	96.23	-	3.32/3.39	[67]
Ag-decorated V_2O_5	93.7	51.7	9.4/13.6	[70]
Ti-doped V_2O_5	95.7	51.1	5/6	[71]
Ti^{4+}-doped V_2O_5 film	34.15	-	9/-	[65]
WO_3 nanosheet/ITO composite	154.16	88	-	[72]
WO_3@PEO fibrous	61.3	-	1.6/-	[73]
WO_3 (pH-tuned film)	122.2	30	1.10/1	[74]
This study	26.53	**37.11**	**7/14**	-

CRediT authorship contribution statement

Faisal Abdullah Sadeq: Methodology, Investigation, Formal analysis, Data curation. **Pei-Ling Low:** Visualization, Supervision, Resources, Project administration, Funding acquisition. **Tan Kar:** Writing – review & editing, Visualization, Validation. **Zhang-Xuan Cheng:** Writing – original draft, Software, Methodology, Investigation, Formal analysis, Data curation. **Ming-Yue Tan:** Methodology, Investigation, Formal analysis. **Cheikh Zakaria Eldjilali:** Methodology, Investigation, Formal analysis. **Ebrahem Abdelhamed Abdelrahman:** Methodology, Investigation, Formal analysis. **Kah-Yoong Chan:** Writing – review & editing, Visualization, Validation, Supervision, Resources, Project administration, Investigation, Funding acquisition, Formal analysis, Conceptualization. **Thien Gregory:** Writing – original draft, Software, Methodology, Investigation, Formal analysis, Data curation.

Funding

We would like to acknowledge Telekom Research & Development Sdn Bhd for financial sponsorship through TM R&D Grant 2023 (Grant No: RDTC/231080, Project ID: MMUE/230009) and TM R&D Grant 2026.

Declaration of Competing Interest

The authors declare the following financial interests/personal relationships which may be considered as potential competing interests: Kah-Yoong Chan reports financial support was provided by Universiti Multimedia - Kampus Cyberjaya. If there are other authors, they declare that they have no known competing financial interests or personal relationships that could have appeared to influence the work reported in this paper.

Acknowledgments

The funding for the APC was provided by Telekom Malaysia Research and Development (TM R&D).

Data availability

Data will be made available on request.

References

[1] T.H. Wang, S.C. Jeng, An active and passive controllable smart glass based on an eco-friendly aqueous solution, Adv. Mater. Technol. 9 (2024), https://doi.org/10.1002/admt.202301396.

[2] C.Y. Jeong, T. Kubota, K. Tajima, Flexible electrochromic devices based on tungsten oxide and Prussian blue nanoparticles for automobile applications, RSC Adv. 11 (2021), https://doi.org/10.1039/d1ra05280b.

[3] L. Zhang, C. Pan, H. Zeng, K. Han, Y. Gao, Amorphous and porous C/N-doped NiO for electrochromic smart windows applications, Opt. Mater. 167 (2025) 117338, https://doi.org/10.1016/J.OPTMAT.2025.117338.

[4] M. Zhang, J. Fu, N. Xu, L. Meng, A dual-modification strategy for both the Quinone-based cathode and Zn anode electrodes of the aqueous zinc-ion battery, Chem. Eng. J. 511 (2025) 161944, https://doi.org/10.1016/J.CEJ.2025.161944.

[5] Y. Wei, J. Zhou, J. Zheng, C. Xu, Improved stability of electrochromic devices using Ti-doped V2O5 film, Electro Acta 166 (2015), https://doi.org/10.1016/j.electacta.2015.03.087.

[6] T. Dhandayuthapani, R. Sivakumar, D. Zheng, H. Xu, R. Ilangovan, C. Sanjeeviraja, J. Lin, WO3/TiO2 hierarchical nanostructures for electrochromic applications, Mater. Sci. Semicond. Process 123 (2021), https://doi.org/10.1016/j.mssp.2020.105515.

[7] Handbook of Inorganic Electrochromic Materials, 1995. https://doi.org/10.1016/b978-0-444-89930-9.x5000-4.

[8] J. Chen, Z. Wang, Z. Chen, S. Cong, Z. Zhao, Fabry-perot cavity-type electrochromic supercapacitors with exceptionally versatile color tunability, Nano Lett. 20 (2020), https://doi.org/10.1021/acs.nanolett.9b05152.

[9] A.H.E. Abdelhamed, K.Y. Chan, B.W.C. Au, G.S.H. Thien, P.L. Low, Y.K. Sin, C. L. Lee, W.L. Pang, Electrochromic properties of sol-gel deposited electrochromic TiO2 thin films, J. Adv. Res. Appl. Sci. Eng. Technol. 31 (2023), https://doi.org/10.37934/araset.31.2.7180.

[10] I. Mjejri, M. Gaudon, A. Rougier, Mo addition for improved electrochromic properties of V2O5 thick films, Sol. Energy Mater. Sol. Cells 198 (2019), https://doi.org/10.1016/j.solmat.2019.04.010.

[11] D. Tadeu Cestarolli, E.Maria Guerra, Vanadium pentoxide (V2O5): their obtaining methods and wide applications. Transition Metal Compounds Synthesis Properties Application, 2021.

[12] M. Benmoussa, A. Outzourhit, R. Jourdani, A. Bennouna, E.L. Ameziane, Structural, optical and electrochromic properties of Sol–Gel V2O5 thin films, Act. Passiv. Electron. Compon. 26 (2003) 245–256, https://doi.org/10.1080/0882751031000116223.

[13] N.S. Pham, Y.H. Seo, E. Park, T.D.D. Nguyen, I.S. Shin, Implementation of high-performance electrochromic device based on all-solution-fabricated Prussian blue and tungsten trioxide thin film, Electro Acta 353 (2020), https://doi.org/10.1016/j.electacta.2020.136446.

[14] B.W.C. Au, K.Y. Chan, G.S.H. Thien, M.E. Yeoh, M.Z. Sahdan, H.C.A. Murthy, The Effect of Transparent Conducting Oxide Films on WO3-Based Electrochromic Devices with Conducting Polymer Electrolytes, Polymers 15 (2023), https://doi.org/10.3390/polym15010238.

[15] A.Hamed Ebrahem Abdelhamed, G.Soon How Thien, C.-L. Lee, B.Wen-Cheun Au, K.Ban Tan, H.C.Ananda Murthy, K.-Y. Chan, Solution Casting Effect of PMMA-Based Polymer Electrolyte on the Performances of Solid-State Electrochromic Devices, (2025). https://doi.org/10.3390/polym17010099.

[16] L.H. Cardozo Amorin, L. Da Silva Martins, F. Lopes, A. Urbano, Thickness effect on the optical band gap of V2O5 thin films deposited by thermal evaporation, Semin. Ciências Exatas e Tecnol. ógicas 38 (2018) 59, https://doi.org/10.5433/1679-0375.2017V38N2P59.

[17] M. Panagopoulou, D. Vernardou, E. Koudoumas, D. Tsoukalas, Y.S. Raptis, Tungsten doping effect on V2O5 thin film electrochromic performance, Electro Acta 321 (2019), https://doi.org/10.1016/j.electacta.2019.134743.

[18] A. Mauger, C.M. Julien, V 2 O 5 thin films for energy storage and conversion, (2018). https://doi.org/10.3934/matersci.2018.3.349.

[19] Y. Liu, S. Zhu, Y. Su, R. Chen, W. Zhang, X. Niu, W. Chen, X. Chen, Z. An, Solution-type electrochromic devices based on D-π-D thiophene derivatives, Mater. Today Commun. 33 (2022) 104910, https://doi.org/10.1016/J.MTCOMM.2022.104910.

[20] G.Y. Zhang, L.L. Ma, E. Lin, Z.Y. Wang, J.T. Pan, J. Yang, M. Deng, Y. Wei, Y. Ye, N. Wang, Y. Wang, S. Aya, Y.Q. Lu, Periodically-modulated unipolar and bipolar orders in nematic fluids towards miniaturized nonlinear vectorial optics, Nat. Commun. 2025 16 (1) (2025) 9419, https://doi.org/10.1038/s41467-025-64463-2.

[21] E. Wu, Y. Ma, Q. Tian, Z. Wang, Z. Song, S. Huo, F. Meng, Y. Xie, C. Pan, W-Shaped antiambipolar transistors based on h-BN/MoTe2/BP heterostructures, ACS Nano 19 (2025) 35701–35711, https://doi.org/10.1021/ACSNANO.5C11809.

[22] M.Y. Tan, G.S.H. Thien, K.B. Tan, H.C.A. Murthy, K.Y. Chan, Investigation of electrochromic performances of multicolor V2O5 devices fabricated at low processing temperature, Sci. Rep. 2025 15 (1) (2025) 1–14, https://doi.org/10.1038/s41598-024-85014-7.

[23] R. Amrani, E. Garoudja, F. Lekoui, W. Filali, H. Neggaz, Y.A. Djebeli, L. Henni, S. Hassani, F. Kezzoula, S. Oussalah, F. Al mashary, M. Henini, Investigation of structural and electrical properties of ITO thin films and correlation to optical parameters extracted using novel method based on PSO algorithm, Bull. Mater. Sci. 2023 46 (1) (2023) 1–11, https://doi.org/10.1007/S12034-022-02845-8.

[24] S. Alghool, H.F. Abd El-Halim, A.M. Mostafa, An eco-friendly synthesis of V2O5 nanoparticles and their catalytic activity for the degradation of 4-nitrophrnol, J. Inorg. Organomet Polym. Mater. 29 (2019), https://doi.org/10.1007/s10904-019-01096-1.

[25] T.K. Le, M. Kang, V.T. Tran, S.W. Kim, Relation of photoluminescence and sunlight photocatalytic activities of pure V2O5 nanohollows and V2O5/RGO nanocomposites, Mater. Sci. Semicond. Process 100 (2019), https://doi.org/10.1016/j.mssp.2019.04.047.

[26] S. Fatimah, R. Ragadhita, D.F.Al Husaeni, A.B.D. Nandiyanto, How to calculate crystallite size from X-ray diffraction (XRD) using Scherrer method, ASEAN J. Sci. Eng. 2 (2022) 65–76, https://doi.org/10.17509/AJSE.V2I1.37647.

[27] V. Kaushik, K. Bhardwaj, D. Kumar, M. Kumar, S.K. Sharma, Effect of various processing parameters on the properties of ZnO thin films, Hybrid. Adv. 7 (2024) 100295, https://doi.org/10.1016/J.HYBADV.2024.100295.

[28] T. Park, K. Kim, J. Hong, Effects of drying temperature and molar concentration on structural, optical, and electrical properties of β-ga2o3 thin films fabricated by sol–gel method, Coatings 2021 11 (2021) 1391, https://doi.org/10.3390/COATINGS11111391.

[29] M. Dutta, S. Mridha, D. Basak, Effect of sol concentration on the properties of ZnO thin films prepared by sol-gel technique, Appl. Surf. Sci. 254 (2008), https://doi.org/10.1016/j.apsusc.2007.10.009.

[30] B. Wen-Cheun Au, K.Y. Chan, D. Knipp, Effect of film thickness on electrochromic performance of sol-gel deposited tungsten oxide (WO3), Opt. Mater. (Amst.) 94 (2019), https://doi.org/10.1016/j.optmat.2019.05.051.

[31] A.C. Amala, R. Sivakumar, Effect of precursor solution concentration on the properties of spin coated V2O5 thin films, Ceram. Int. 51 (2025) 49986–49997, https://doi.org/10.1016/J.CERAMINT.2025.08.236.

[32] E. Blanco, M. Domínguez, J.M. González-Leal, E. Márquez, J. Outón, M. Ramírez-del-Solar, Insights into the annealing process of sol-gel TiO2 films leading to anatase development: The interrelationship between microstructure and optical properties, Appl. Surf. Sci. 439 (2018) 736–748, https://doi.org/10.1016/J.APSUSC.2018.01.058.

[33] T. Kim, S. Lee, Y.W. Lee, D. Kim, Y. Yun, J.H. Bae, H. Lee, J. Park, Optimizing annealing temperature for enhanced electrical performance and stability of solution-processed In2O3 thin-film transistors, Micromachines 16 (2025) 1091, https://doi.org/10.3390/MI16101091/S1.

[34] A.H. Haritha, M.E. Cruz, O. Sisman, A. Duran, D. Galusek, J.J. Velázquez, Y. Castro, Influence of annealing temperature on the photocatalytic efficiency of sol-gel dip-coated ZnO thin films in methyl orange degradation, Open Ceram. 21 (2025) 100727, https://doi.org/10.1016/J.OCERAM.2024.100727.

[35] N. Kaczmarczyk, J. Szczurek, B. Babiarczuk, P. Gronowicz, M. Paszkowski, M. Kowalski, B. Borak, W. Jones, J. Detyna, J. Krzak, Thin film quality of sol–gel SiO2 coatings prepared on Ti6Al4V depending on their composition and titanium substrate preparation, J. Mater. Sci. 2025 60 (32) (2025) 13974–14004, https://doi.org/10.1007/S10853-025-11273-Y.

[36] G. Song, I. Mjejri, M. Gaudon, A. Rougier, Multi-color electrochromism in vanadium oxide thin films, ECS Meet. Abstr. (2017), https://doi.org/10.1149/ma2017-01/40/1851.

[37] S. Khokhar, H. Anand, P. Chand, Current advances of nickel based metal organic framework and their nanocomposites for high performance supercapacitor applications: a critical review, J. Energy Storage 56 (2022), https://doi.org/10.1016/j.est.2022.105897.

[38] K.E. Macarthur, A.B. Yankovich, A. Béché, M. Luysberg, H.G. Brown, S.D. Findlay, M. Heggen, L.J. Allen, Optimizing experimental conditions for accurate quantitative energy-dispersive X-ray analysis of interfaces at the atomic scale, Microsc. Microanal. 27 (2021) 528–542, https://doi.org/10.1017/S1431927621000246.

[39] W.W.W. Fan, A.F. Gualtieri, A. Hamilton, J.P. Patel, J.A. Salmond, Determining factors affecting the accuracy of SEM-EDX data-based quantitative chemical analysis for identifying naturally occurring individual carcinogenic erionite fibers, Sci. Rep. 2025 15 (1) (2025) 25316, https://doi.org/10.1038/s41598-025-09551-5.

[40] K.F. Lin, H.M. Cheng, H.C. Hsu, L.J. Lin, W.F. Hsieh, Band gap variation of size-controlled ZnO quantum dots synthesized by sol-gel method, Chem. Phys. Lett. 409 (2005) 208–211, https://doi.org/10.1016/J.CPLETT.2005.05.027.

[41] Z. Duan, J. Xu, Effects of sol concentration on the structure and magnetic properties of sol-gel MnZn ferrites, Integr. Ferroelectr. 190 (2018), https://doi.org/10.1080/10584587.2018.1457344.

[42] N.F. Mott, E.A. Davis, K. Weiser, Electronic processes in non-crystalline materials, Phys. Today 25 (1972), https://doi.org/10.1063/1.3071145.

[43] R. Rathika, M. Kovendhan, D.P. Joseph, R. Pachaiappan, A.S. Kumar, K. Vijayarangamuthu, C. Venkateswaran, K. Asokan, S.J. Jeyakumar, Tailoring the properties of spray deposited V2O5 thin films using swift heavy ion beam irradiation, Nucl. Eng. Technol. 52 (2020) 2585–2593, https://doi.org/10.1016/J.NET.2020.04.013.

[44] F.N. Dultsev, L.L. Vasilieva, S.M. Maroshina, L.D. Pokrovsky, Structural and optical properties of vanadium pentoxide sol–gel films, Thin Solid Films 510 (2006) 255–259, https://doi.org/10.1016/J.TSF.2005.12.264.

[45] M.Y. Tan, K.Y. Chan, G.S.H. Thien, K.B. Tan, H.C.A. Murthy, B.W.C. Au, Optical and structural properties of V2O5 electrochromic thin films, J. Eng. Technol. Appl. Phys. 6 (2024) 79–83, https://doi.org/10.33093/JETAP.2024.6.2.11.

[46] K.J. Patel, G.G. Bhatt, S.S. Patel, R.R. Desai, J.R. Ray, C.J. Panchal, P. Suryavanshi, V.A. Kheraj, A.S. Opanasyuk, Thickness-dependent electrochromic properties of Amorphous tungsten trioxide thin films, J. Nano Electron. Phys. 9 (2017), https://doi.org/10.21272/jnep.9(3).03040.

[47] B. Zhang, G. Xu, S. Tan, C. Liu, J. Zhang, Study on electrochromic properties of TiO2 films under Co ion content fluctuations, Opt. Mater. 100 (2020), https://doi.org/10.1016/j.optmat.2020.109659.

[48] V.H.V. Quy, I.R. Jo, S.H. Kang, K.S. Ahn, Amorphous-crystalline dual phase WO3 synthesized by pulsed-voltage electrodeposition and its application to

electrochromic devices, J. Ind. Eng. Chem. 94 (2021), https://doi.org/10.1016/j.jiec.2020.10.047.
[49] M.Y. Tan, K.Y. Chan, C.Z. Eldjilali, A.H.E. Abdelhamed, G. Soon How Thien, B.W. C. Au, B.T. Goh, H.C.A. Murthy, Rapid post-annealing effect on the TiO2-based electrochromic films, Opt. Mater. 145 (2023), https://doi.org/10.1016/j.optmat.2023.114455.
[50] A. Verma, A. Basu, A.K. Bakhshi, S.A. Agnihotry, Structural, optical and electrochemical properties of sol-gel derived TiO2 films: annealing effects, Solid State Ion. 176 (2005), https://doi.org/10.1016/j.ssi.2005.06.011.
[51] A. Abudula, F. Gao, T. Liu, Y. Zhang, M. Song, N. Li, S. Liu, P. Tuersun, Effect of Ag film thickness on the morphology and light scattering properties of Ag nanoparticles, Nanosci. Nanotechnol. Lett. 6 (2014), https://doi.org/10.1166/nnl.2014.1769.
[52] W. Azouzi, H. Ez-Zahraouy, M. Benaissa, H. Labrim, B. Belhorma, M.R. Bricha, B. Jaber, Simple preparation of high transparent tin dioxide thin films by spin coating method: Effect of sol concertation. Proceedings of 2016 International Renewable and Sustainable Energy Conference, IRSEC, 2016, p. 2017, https://doi.org/10.1109/IRSEC.2016.7983926.
[53] R.T. Wen, C.G. Granqvist, G.A. Niklasson, Eliminating degradation and uncovering ion-trapping dynamics in electrochromic WO 3 thin films, Nat. Mater. 14 (2015), https://doi.org/10.1038/nmat4368.
[54] M.H. Kim, H.W. Choi, K.H. Kim, Thickness dependence of WO3-x thin films for electrochromic device application, Mol. Cryst. Liq. Cryst. 598 (2014) 54–61, https://doi.org/10.1080/15421406.2014.933298;WGROUP:STRING:PUBLICATION.
[55] Y. Zhen, B.P. Jelle, T. Gao, Electrochromic properties of WO3 thin films: the role of film thickness, Anal. Sci. Adv. 1 (2020) 124–131, https://doi.org/10.1002/ANSA.202000072;REQUESTEDJOURNAL:JOURNAL:26285452;CTYPE:STRING:JOURNAL.
[56] A.J. More, R.S. Patil, D.S. Dalavi, S.S. Mali, C.K. Hong, M.G. Gang, J.H. Kim, P. S. Patil, Electrodeposition of nano-granular tungsten oxide thin films for smart window application, Mater. Lett. 134 (2014), https://doi.org/10.1016/j.matlet.2014.07.059.
[57] P.J. Morankar, R.U. Amate, N.A. Ahir, C.W. Jeon, Revealing enhanced optical modulation and coloration efficiency in nanogranular WO3 thin films through precursor concentration modifications, Crystals 2024 14 (2024) 915, https://doi.org/10.3390/CRYST14110915.
[58] S.N. Alamri, A.A. Joraid, Smart windows with different thicknesses of V2O5 as ion storage layers, Mater. Sci. Forum 663–665 (2011) 743–750, https://doi.org/10.4028/WWW.SCIENTIFIC.NET/MSF.663-665.743.
[59] K. Srikanth, M.M. Rahman, H. Tanaka, K.M. Krishna, T. Soga, M.K. Mishra, T. Jimbo, M. Umeno, Investigation of the effect of sol processing parameters on the photoelectrical properties of dye-sensitized TiO2 solar cells, Sol. Energy Mater. Sol. Cells 65 (2001), https://doi.org/10.1016/S0927-0248(00)00092-1.
[60] Z. Tong, J. Hao, K. Zhang, J. Zhao, B.L. Su, Y. Li, Improved electrochromic performance and lithium diffusion coefficient in three-dimensionally ordered macroporous V2O5 films, J. Mater. Chem. C. Mater. 2 (2014) 3651–3658, https://doi.org/10.1039/C3TC32417F.
[61] J. Scarminio, P.R. Catarini, A. Urbano, R.V. Gelamo, F.P. Rouxinol, M.A.Bica De Moraes, Li diffusion and electrochromism in amorphous and crystalline vanadium oxide thin film electrodes, J. Braz. Chem. Soc. 19 (2008) 788–794, https://doi.org/10.1590/S0103-50532008000400025.
[62] T. Ahmed, A. Mazumder, S. Kuriakose, A. Dubey, A. Elbourne, J. Ren, V. Krishnamurthi, E. Kandare, I.H. Abidi, E. Della Gaspera, S. Balendhran, S. Walia, Materials, mechanisms, and emerging applications of electrochromic systems, Nanoscale 17 (2025) 18049–18076, https://doi.org/10.1039/D4NR02098G.
[63] A.H.E. Abdelhamed, K.Y. Chan, B.W.C. Au, G.S.H. Thien, P.L. Low, Y.K. Sin, C. L. Lee, W.L. Pang, Electrochromic properties of Sol-Gel deposited electrochromic TiO2 thin films, J. Adv. Res. Appl. Sci. Eng. Technol. 31 (2023) 71–80, https://doi.org/10.37934/ARASET.31.2.7180.
[64] J. Guo, H. Jia, Z. Shao, P. Jin, X. Cao, Fast-switching WO3-based electrochromic devices: design, fabrication, and applications, Acc. Mater. Res. 4 (2023), https://doi.org/10.1021/accountsmr.2c00217.
[65] Y. Deng, H. Li, J. Liang, J. Liao, M. Huang, R. Chen, Y. Long, J. Robichaud, Y. Djaoued, Excellent electrochromic properties of Ti4+-induced nanowires V2O5 films, Materials 17 (2024), https://doi.org/10.3390/MA17194680.
[66] Y. Wei, J. Zhou, J. Zheng, C. Xu, Improved stability of electrochromic devices using Ti-doped V2O5 film, Electro Acta 166 (2015) 277–284, https://doi.org/10.1016/J.ELECTACTA.2015.03.087.
[67] B.K. Mandlekar, A.L. Jadhav, A. Pol, A.V. Kadam, Vacancy-defect assisted electrochromic applications in V2O5 nanomaterials, Discov. Electrochem. 2 (2025) 1–19, https://doi.org/10.1007/S44373-025-00050-W.
[68] C.E. Patil, N.L. Tarwal, P.R. Jadhav, P.S. Shinde, H.P. Deshmukh, M.M. Karanjkar, A.V. Moholkar, M.G. Gang, J.H. Kim, P.S. Patil, Electrochromic performance of the mixed V2O5–WO3 thin films synthesized by pulsed spray pyrolysis technique, Curr. Appl. Phys. 14 (2014) 389–395, https://doi.org/10.1016/J.CAP.2013.12.014.
[69] M.Y. Tan, G.S.H. Thien, K.B. Tan, H.C.A. Murthy, K.Y. Chan, Investigation of electrochromic performances of multicolor V2O5 devices fabricated at low processing temperature, Sci. Rep. 15 (2025), https://doi.org/10.1038/S41598-024-85014-7.
[70] M.A. Çarpan, O. Şentürk, S.R. Tokgöz, S. Sarsıcı, S.K. Akay, A. Peksöz, Ag decorated V2O5 electrodes as a promising option for electrochromic, photovoltaic, and energy-saving applications, Ceram. Int. 50 (2024) 33111–33122, https://doi.org/10.1016/J.CERAMINT.2024.06.121.
[71] Y. Lu, L. Liu, D. Mandler, P.S. Lee, High switching speed and coloration efficiency of titanium-doped vanadium oxide thin film electrochromic devices, J. Mater. Chem. C. Mater. 1 (2013) 7380–7386, https://doi.org/10.1039/C3TC31508H.
[72] F.H. An, Y.Z. Yuan, J.Q. Liu, M.D. He, B. Zhang, Enhanced electrochromic properties of WO3/ITO nanocomposite smart windows, RSC Adv. 13 (2023) 13177, https://doi.org/10.1039/D3RA01428B.
[73] H. Kwon, S. Kim, M. Ham, Y. Park, H. Kim, W. Lee, H. Lee, Enhanced Coloration Time of Electrochromic Device Using Integrated WO 3 @PEO Electrodes for Wearable Devices, (2023). https://doi.org/10.3390/bios13020194.
[74] A. Khan, S.N. Sapakal, A. Kadam, Tailoring tungsten trioxide (WO3): pH-dependent synthesis, structural insights, and exceptional electrochromic performance, Sustainability 5 (2025) 100065, https://doi.org/10.1016/J.NXSUST.2024.100065.